Available online at www.sciencedirect.com

SCIENCE DIRECT

Cement and Concrete Research 35 (2005) 1948 – 1960

Cement and Concrete Research

Modeling the linear elastic properties of Portland cement paste

C.-J. Haecker[d,1], E.J. Garboczi[a,*], J.W. Bullard[a], R.B. Bohn[b], Z. Sun[c], S.P. Shah[c], T. Voigt[c]

[a]National Institute of Standards and Technology, Materials and Construction Research Division, Gaithersburg, MD 20899, United States
[b]National Institute of Standards and Technology, Mathematical and Computational Sciences Division, Gaithersburg, MD 20899, United States
[c]Northwestern University, Department of Civil Engineering, Evanston, IL 60208, United States
[d]SE Tylose GmbH and Co. KG (Shin-Etsu), 65203 Wiesbaden, Germany

Received 6 March 2005; accepted 1 May 2005

Abstract

The linear elastic moduli of cement paste are key parameters, along with the cement paste compressive and tensile strengths, for characterizing the mechanical response of mortar and concrete. Predicting these moduli is difficult, as these materials are random, complex, multi-scale composites. This paper describes how finite element procedures combined with knowledge of individual phase moduli are used, in combination with a cement paste microstructure development model, to quantitatively predict elastic moduli as a function of degree of hydration, as measured by loss on ignition. Comparison between model predictions and experimental results are good for degrees of hydration of 50% or greater, for a range of water : cement ratios. At early ages, the resolution of the typical 100^3 digital microstructure is inadequate to give accurate results for the tenuous cement paste microstructure that exists at low degrees of hydration. Elastic computations were made on higher resolution microstructures, up to 400^3, and compared to early age elastic moduli data. Increasing agreement with experiment was seen as the resolution increased, even when ignoring possible viscoelastic effects.
Published by Elsevier Ltd.

Keywords: Hydration; Microstructure; Elastic moduli; Modeling

1. Introduction

The mechanical properties of cement-based materials are almost always of primary importance in material applications since concrete, by far the largest volume use of these materials, is mainly used as a structural material. The mechanical properties of interest are threefold: short-term deflection, which is controlled by the elastic properties; long-term deflection, which is controlled by the viscoelastic properties; and failure, which is controlled by the strength. If failure is in compression, then we are concerned with the compressive strength; if in tension, we are concerned with the tensile strength.

In this paper, we will only discuss the elastic properties, and will assume that cement paste is a linear elastic material. For a linear elastic material, mathematically the stress, σ_{ij}, is related to the strain, ε_{kl}, via the elastic modulus tensor, C_{ijkl}: $\sigma_{ij} = C_{ijkl}\ \varepsilon_{kl}$. Since we are only considering small strains, small with respect to strains at failure, we can ignore failure. Cement-based materials are much more viscoelastic at early ages than at later ages [1]. At ages of 14 d or older, cement paste is well-approximated as a linear elastic material [1], at least for short loading times.

Theoretically predicting the elastic moduli of concrete is a difficult task. First, at the millimeter scale, concrete is a complex, random composite, because of a high loading of a wide size range of fine and coarse aggregates, with all the theoretical difficulties that involves [2–4]. But the cement paste matrix itself is an even more complex, random composite at the micrometer scale. And of course, the main physical phase of cement paste, the calcium–silicate–hydrate (C–S–H)[2] phase, is a random complex composite at the nanometer scale. So correctly predicting the elastic

* Corresponding author.
E-mail address: edward.garboczi@nist.gov (E.J. Garboczi).
[1] Formerly at Dyckerhoff AG, Wiesbaden, Germany.

[2] Standard cement chemistry notation is used: C=CaO, S=SiO_2, A=Al_2O_3, F=Fe_2O_3, H=H_2O, K=K_2O and S=SO_3.

0008-8846/$ - see front matter. Published by Elsevier Ltd.
doi:10.1016/j.cemconres.2005.05.001

moduli of concrete, based on knowledge of individual phases, is a multi-scale problem [5,6]. In this paper, we focus on computing the elastic moduli of cement paste at the micrometer scale, by taking into account all the microstructure at that scale but treating the C–S–H phase as an elastically homogeneous phase. Theoretical predictions are compared quantitatively with experimental results.

2. Cement paste computer models

Computing cement paste elastic moduli involves three tasks, no matter what techniques are used: (1) having a proper microstructure (porosity, arrangement of solids), (2) recognizing their differences and using the proper elastic moduli for each solid phase, and (3) combining (1) and (2) together mathematically in some reasonable fashion. This section discusses how we handle tasks (1) and (3). How we have obtained values for task (2) is discussed in the next section.

To numerically determine the cement paste microstructure at the micrometer level, the program CEMHYD3D was used [7]. This program starts with a careful chemical analysis of cement particles, so that statistically, the chemical phase makeup of individual particles, as well as bulk volume fractions, are determined. The percolation properties of this model have recently been updated [8]. Model 3-D particles are made from this information (either spherical or real particle shapes [9,10]) and incorporated into a 3-D digital computational box according to the known particle size distribution and water:cement mass ratio. Model hydration is carried out via cycles of dissolution, diffusion, and reaction, according to known reaction equations. The correct volumetric stoichiometry is maintained throughout the hydration modeling process. The finest cement particles are usually smaller than the smallest particle possible in the digital microstructure, one voxel. The volume associated with these particles are lumped into the volume for the one-voxel particles. Recent analysis has shown how the effect of the size of these small particles can be quantitatively incorporated into the hydration model via a curvature-based dissolution bias [11]. The results in this paper do not include such a bias, which only can affect the early age results [11]. The output is a 3-D digital microstructure, where each voxel is labeled as belonging to a single phase. The degree of hydration is easily computed for each of these microstructures by simply counting the amount of unreacted cement and comparing it to the initial amount present before hydration.

These microstructures are then taken and used as input into a computer code called *elas3d.f* [12,13]. This program treats each cubic voxel as a tri-linear finite element, upon which the elastic equations are discretized and solved using a relaxation algorithm [14]. The average stress for a given strain is used to determine the composite moduli, which are averaged over direction to minimize the effects of having a small, periodic model of a large microstructure. This program has been used successfully for several other materials, including tungsten–silver composites [15], porous ceramics [16], hydrated gypsum plaster-like models in 2- and 3-D [17], model open- and closed-cell foams [18,19], sedimentary rocks [20], and leached cement paste [21]. A review of the application of this computer program to a wide range of model materials is available [22]. Within the limits of the resolution of the original image, the program checks out well against exact solutions [12] and experimental data [18,19,21].

The elas3d.f program is essentially an elastic solver for composite materials. Given a correct arrangement of phases, correct elastic moduli for individual phases, and a reasonable resolution, the program will give an accurate result for the overall composite moduli. As was said above, CEMHYD3D is used to give the microstructure. The next section describes how individual phase elastic moduli were obtained.

3. Individual phase properties of cement paste

The elastic modulus tensor of an isotropic elastic material has only two independent values, which are usually given as any two of the set: the Young's modulus, E, the Poisson's ratio, v, the bulk modulus, K, and the shear modulus, G. The following equations show the relationship between these parameters [23,24]:

$$\frac{9}{E}=\frac{1}{K}+\frac{3}{G} \qquad v=\frac{(3K-2G)}{2(3K+G)}$$
$$K=\frac{E}{3(1-2v)} \qquad G=\frac{E}{2(1+v)} \tag{1}$$

These equations are given because different sources for the elastic moduli of individual phases are given in terms of different combinations of these parameters.

Some individual cement and cement paste phase elastic properties can be found in the geological literature, as they are crystalline minerals found in nature whose elastic properties have been measured. In general, the elastic moduli of a single crystal will give an anisotropic elastic moduli tensor reflecting the symmetry of the crystal lattice. An isotropic average can be performed on this tensor, which will result in an isotropic average elastic modulus tensor (two independent elastic moduli). Two ways in which this can be done, called the Voigt and Reuss averages [25,26], respectively, result in an upper bound and a lower bound. The average of these bounds for various cement and cement paste phases are reported in Table 1. This isotropic tensor should be more representative of what appears in real cement paste, where the crystalline phases are polycrystalline and randomly dispersed. For the sake of completeness, all four of the elastic moduli are reported in Table 1. A tighter set of bounds for the averaged moduli can be generated, the Hashin bounds

Table 1
Elastic moduli of individual cement and cement paste phases, taken from several sources in the literature

Cement chemistry notation	Mineral name	K (GPa)	G (GPa)	E (GPa)	υ	Ref.
H	Water	2.2	0.0	–	–	[27]
C_3S	Tricalcium silicate	105.2	44.8	117.6	0.314	[34]
C_2S	Dicalcium silicate	Same as C_3S				[35]
C_3A	Tricalcium aluminate	Same as C_3S				[35]
C_4AF	Tetracalcium aluminoferrite	Same as C_3S				[35]
$C\overline{S}\cdot H_2 (gypsum)$	Dihydrate	42.5	15.7	45.7	0.33	[28,29]
$C\overline{S}\cdot H_{1/2}$	Hemihydrate	52.4	24.2	62.9	0.30	
$C\overline{S}$	Anhydrite	54.9	29.3	80.0	0.275	[28,29]
$K\overline{S}$	Potassium sulfate (arcanite)	31.9	17.4	44.2	0.269	[28,29]
$N\overline{S}$	Sodium sulfate (thenardite)	43.4	22.3	57.1	0.281	[28,29]
SiO_2	Silica fume	36.5	31.2	72.8	0.167	[31]
CH	Portlandite	40.0	16.0	42.3	0.324	[32,33]
$C_{1.7}SH_4$	C–S–H	14.9	9.0	22.4	0.25	[5,38]
$CaCO_3$	Limestone	69.8	30.4	79.6	0.31	[28,29]
C_3AH_6	Hydrogarnet	Same as C–S–H				
$C_6A\overline{S}_3H_{32}$	Ettringite	Same as C–S–H				
$C_4A\overline{S}H12 (Afm)$	Monosulfate	Same as CH				
FH_3	Iron hydroxide	Same as C–S–H				
$CaCl_2$	Calcium chloride	Same as CH				
$C_3A(CaCl_2)H_{10}$	Friedel salt	Same as ettringite				
C_2ASH_8	Stratlingite	Same as C–S–H				
$C_3A(CaCO_3)H_{11}$ (Afmc)	Monocarbonate	Same as Afm				

[25,26], but the average of these compares quite closely with the average of the Voigt–Reuss bounds. The Voigt–Reuss bounds are much simpler mathematically, so these are used in Table 1. Refs. [27–31] are general compilations of the elastic properties of various minerals, usually given in terms of averages of the Voigt–Reuss bounds, not the full anisotropic elastic tensor.

The elastic moduli of some cement/cement paste phases, phases not usually found in nature, have been reported in journal articles. The full anisotropic elastic tensor has been measured for calcium hydroxide (CH) via Brillouin scattering [32], and the Hashin bounds have been computed [33]. The average of the Hashin bounds is what is listed in Table 1. The polycrystalline isotropic elastic moduli of fully dense hot-pressed powder compacts of C_3S have been measured [34], and are listed in Table 1. The Young's moduli of the other clinker phases, C_2S, C_3A, and C_4AF, have been measured via nano-indentation [35], which have shown that the Young's modulus of these phases, including C_3S, are all about the same, certainly within 15%. For simplicity, and since the moduli of C_3S have been previously measured carefully, these values are used for all of the clinker phases in the model reported in this paper.

Because of their volumetric abundance, the three phases that play the largest role in determining cement paste elastic moduli are clinker, CH, and C–S–H. The Young's modulus of late age C–S–H can be estimated from well-hydrated systems [36] to be about 25 GPa. The Poisson's ratio is estimated to be about 0.25. Nano-indentation has recently been used to measure the Young's modulus of C–S–H [5]. A bi-modal distribution of Young's modulus values was found, which accords with the hypothesized two kinds of C–S–H present in cement paste [37]. When averaged together, a value of $E=23.8$ GPa was found [5]. A value of 0.24 for Poisson's ratio was assumed. These numbers accord well with the estimates made above, and with other nano-indentation results [38]. In this paper, the elastic moduli values taken for C–S–H were: $E=22.4$ GPa and $\nu=0.25$ (see Table 1). The values for Young's modulus for all three estimates agree within experimental uncertainty. No measurement of the Poisson's ratio of C–S–H has been made at the present time. Measuring the Poisson's ratio with nano-indentation is not an easy task [39], hence the estimate here.

Ettringite is another phase that can appear in some quantity in some cement pastes, but probably only plays a minor elastic role. A recent paper by Zohdi et al. [40] takes measurements made on packed powder compacts and extrapolates them to zero porosity to estimate that the isotropically averaged, polycrystalline elastic moduli of ettringite are $E=52$ GPa and $G=20$ GPa. This extrapolation was complicated mathematically, and gave a very high degree of curvature of the moduli vs. porosity plots at low porosities. The minimum porosity that was actually measured was 23.8%. We have made similar measurements, but on more porosities and on a minimum porosity of about 11%. Both sets of data are shown in Fig. 1. Comparing to the extrapolation made in Ref. [40], our 11% porosity measurement falls well below their extrapolation, which calls into question their extrapolation procedure. At higher porosities, where comparison can be made, the two sets of data agree fairly well, probably within experimental error when taking into account possible differences in compaction. The experimental uncertainty on our measurements was less than 1% for the resonance measurement and about 3–5% for the measurement of the porosity of the ettringite

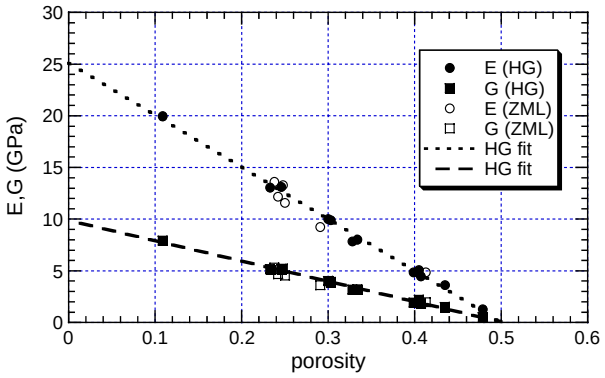

Fig. 1. Two sets of experimental measurements on powder compacts of ettringite. HG=Haecker–Garboczi (this paper), ZML=Zohdi, Monteiro, and Lamour [40].

powder compact. The resonance measurements are actually quite precise, but differences in compaction tend to negate this precision. In Fig. 1 are also shown simple linear fits to all our data, giving a zero porosity value of $E=25$ GPa and $G=10$ GPa. The data of Ref. [40] falls fairly well on these lines. These values for fully dense, polycrystalline ettringite accord well with our values for C–S–H, which is another material that incorporates a large amount of water like ettringite. That is why in Table 1, and in the simulations, the elastic moduli of ettringite were taken to be the same as for C–S–H.

A few other phases in Table 1 are listed as having elastic moduli "same as" another phase. The elastic moduli of these minor phases are not known independently. Hence, the elastic moduli were taken, as a "best guess," to have elastic moduli equal to that of another phase, which phase they most resembled structurally. Also, for hemihydrate gypsum, the E and υ values for this phase, which could not be found in the literature, are just the average of the literature values of dihydrate gypsum and anhydrite gypsum. Other schemes could be proposed, based on the relative water content, but in lieu of data, a simple averaging scheme is just as plausible as a more sophisticated scheme. If a pore space voxel is encountered that has been emptied of water due to self-desiccation, its elastic moduli are both set equal to zero.

The uncertainty in the measured elastic moduli in Table 1 is probably less than 10%, taking into account both measurement uncertainty, the uncertainty in using averaged values instead of full tensor values, as described above, and the difficulties in preparing or finding pure phases. The "best-guess" values for the minor phases must have greater uncertainty, probably in the range of 50–100%.

4. Cement paste results

4.1. Later age materials

Two different cements were chosen to test whether the combination of CEMHYD3D and finite element computations could accurately predict cement paste elastic moduli at later ages. The first cement was denoted D, and was roughly equivalent to an ASTM type I cement. Its composition is given in Table 2 in terms of the major chemical phases present in the cement. This was a finely ground cement, thus showing fast early hydration. The cement particle size distribution (PSD), phase abundance in the cement powder, and amount and forms of gypsum were analyzed so that CEMHYD3D could accurately hydrate this cement and make hydrated microstructures. It is interesting to note that in this cement, the gypsum (volume fraction of 5% of the cement) was mainly in the form of anhydrite (2/3), and hemihydrate (1/3), probably in order to guarantee an optimized strength development. The cement also included a volume fraction of about 5% inert filler, mainly limestone. A second cement, ASTM type I, was denoted H. It was somewhat different chemically from the D cement, as seen in Table 2, and was somewhat coarser. Fig. 2 shows the PSD curves of both cements, displaying the differences in PSD between them. Table 2 and Fig. 2 also show the chemical phase information and PSD, respectively, for a third cement, denoted L, which will be discussed later in Section 4.2. All three cements were analyzed and incorporated into the Virtual Cement and Concrete Testing Laboratory (VCCTL) database, so that microstructures could be generated.

Table 2
Chemical phase composition of the three cements used in this paper (unit is volume fraction of total cement)

Phase	H cement	D cement	L cement
C_3S	0.638	0.705	0.726
C_2S	0.085	0.091	0.048
C_3A	0.049	0.087	0.101
C_4AF	0.077	0.011	0.055
Gypsum	0.025	0	0.07
Hemihydrate	0.024	0.016	0
Anhydrite	0.018	0.036	0
$CaCO_3$	0	0.052	0
Inert	0.084	0	0

Estimated uncertainty in each number is approximately 5%.

Fig. 3 shows the experimental degree of hydration vs. w/c ratio, measured using non-evaporable water content, for

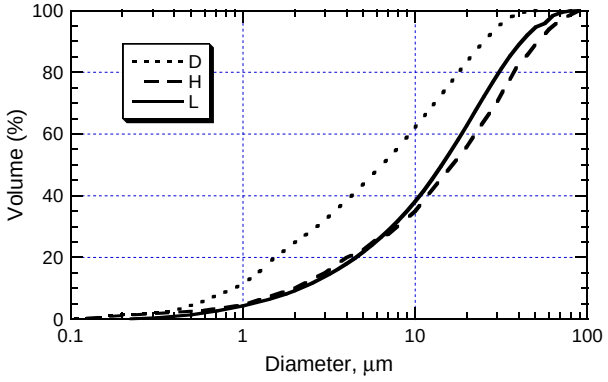

Fig. 2. Cumulative (volume-based) particle size distributions for D, H, and L cements.

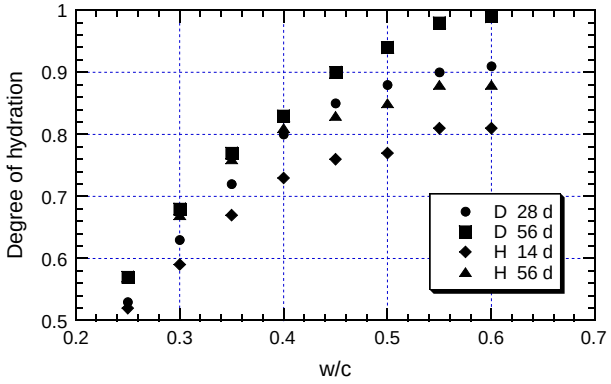

Fig. 3. Degree of hydration vs. w/c for 28 and 56 d results on D cement and 14 d and 56 results for H cement.

28 and 56 d periods of saturated hydration for the D cement and for 14 and 56 d periods of saturated curing for the H cement. Non-evaporable water content is essentially the mass loss between 105 and 1000 °C, which can be used to give a measure of the degree of hydration [7]. These values are an average over three specimens, with an uncertainty ranging from 0.5% to 2.1%. Note that the degree of hydration is higher for the D cement, almost certainly due to the finer particle size. For all systems studied, the degree of hydration was above 50%, although full hydration was not achieved at 56 d. The CEMHYD3D [7] model was run until the model degree of hydration closely matched the experimental degrees of hydration. Then these microstructures were saved for elastic moduli computation.

Fig. 4 shows cross-sections of the 56 d cement D simulated microstructures. Hydration is nearly complete after 56 d. The low w/c ratio pastes are characterized by large amounts of unhydrated clinker phases and very low porosity, while the higher w/c ratio pastes have higher amounts of porosity and almost no clinker phases leftover. So we could say that the low w/c pastes are C–S–H/CH composites reinforced by the stiff clinker phases, while the higher w/c ratio pastes are C–S–H/CH composites made less stiff by pore inclusions. Also, in the lower w/c value microstructures, there is some hint of the original spherical particle shape left for the largest cement particles. Recent CEMHYD3D model improvements have allowed real cement particle shapes to be used in the starting particle microstructure [9]. In composite materials, it is well-known that the shape of the phases can play a large role in determining the overall properties, including elastic behavior [41–43]. Examining the cement paste model microstructures of the H and D cements above revealed that due to cement consumption during hydration, initial cement particle shape would not have played much of a role in the elastic properties of these cement paste systems. However, the remnant spherical particle shapes in the lower w/c pastes imply that there could be a small effect of particle shape even at this late stage of hydration. It is probably true, though, that cement particle shape could play a very large role in determining early age mechanical behavior, as the cement particles will play the role of relatively very stiff inclusions in a quite soft matrix. It is known that the higher the contrast between inclusion and matrix, the more effect the shape of the inclusion has upon composite properties [41–43]. This will be discussed more in the next section.

Fig. 5 shows the experimental and model results for E and G for the D cement, plotted vs. w/c ratio. The experimental results for both cements were obtained via elastic resonance measurements (similar to ASTM E1875-00e1 standard test method for dynamic Young's modulus, Shear modulus, and Poisson's ratio by sonic resonance). In these experiments, E and G were measured directly, so that the model results are presented for the same two parameters. The experimental results are an average over three specimens, with an uncertainty between 0.5% and 0.8%. At each w/c value, the lower value is the 28 d result and the upper value is the 56 d result. There is excellent agreement between model predictions and experimental results, mostly within 5% although up to 10% disagreement for some values. The

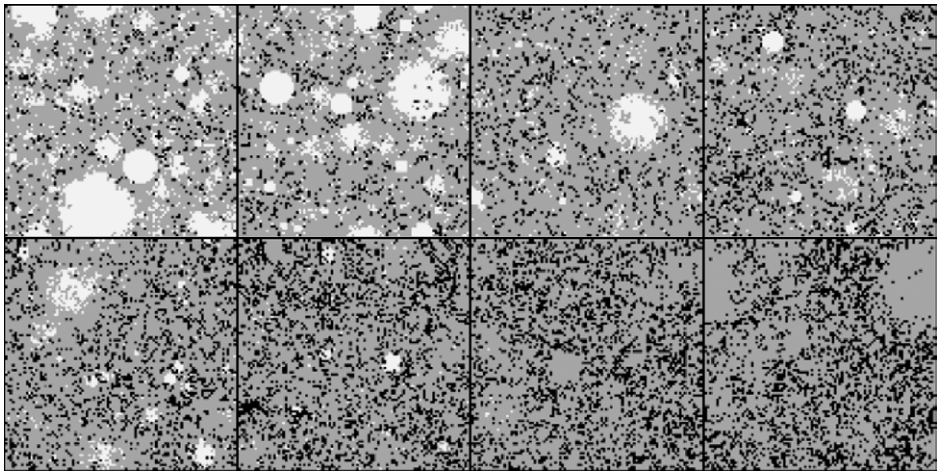

Fig. 4. 56 d D cement paste microstructures (top row, starting from left: w/c=0.25, 0.3, 0.35, 0.4; second row, starting from left: w/c=0.45, 0.5, 0.55, 0.6). White is the unreacted cement particles, black is pore space, and all hydration products are gray.

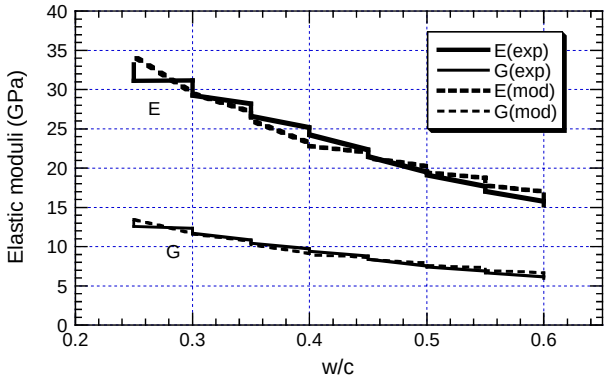

Fig. 5. D cement data, 28 and 56 d results. At each w/c value, the 28 and 56 d elastic moduli values make the curves seem jagged. The 56 d values are always higher than the 28 d values.

cement paste microstructure is isotropic on average, and so a pure shear and hydrostatic compression can be applied at the same time, since any cross terms in the elastic moduli tensor, e.g. C_{1123}, are small compared to the other components within numerical round-off error, and average to zero.

In Fig. 6, the model and experimental results are plotted for (a) 14 d of curing and (b) 56 d of curing for the H cement. The format of the graph is similar to that of Fig. 5, and the experimental uncertainties were similar. The same excellent agreement between experiment and model is demonstrated. At the highest w/c value, some bleeding was noted, which tended to raise the measured elastic moduli values. The model was run for a slightly lower w/c ratio, 0.55 instead of 0.6, and good agreement was obtained for the 0.6 w/c point.

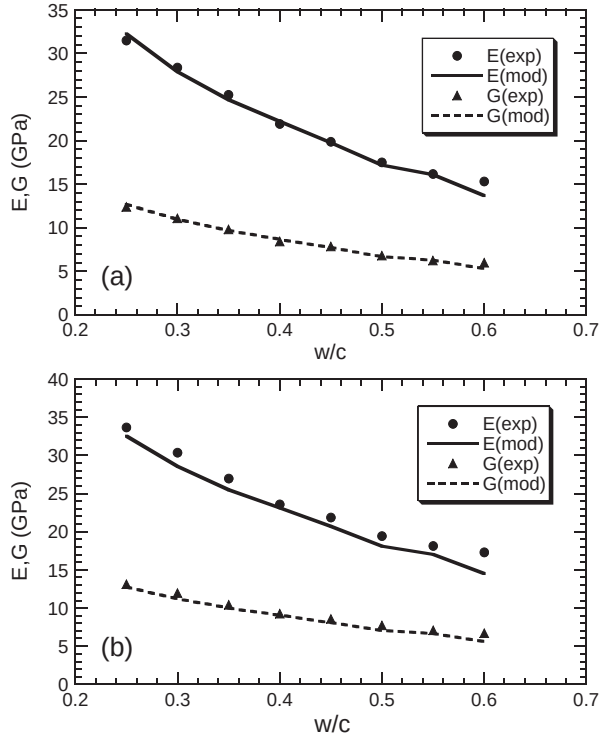

Fig. 6. H cement data. (a) 14 d, (b) 56 d.

4.2. Early age materials

Linear elastic data were collected via a resonant frequency method (ASTM C215-97) for early age cement paste elastic moduli for the L cement. It was found that the computed elastic moduli, using real particle shapes [9], were much too high, compared to experiment, when a 100^3 microstructure was used. Since the early age cement paste microstructure is very tenuous – small amounts of hydration products holding together much stiffer cement particles – it was very possible that higher resolution finite element meshes could be necessary to properly represent this tenuous microstructure. Higher resolution microstructures were made in two ways. First, larger cement particle systems were made, and hydration was carried out at the higher resolution (200^3–0.5 μm/voxel and 400^3–0.25 μm/voxel), which involved some modifications to the CEMHYD3D code [44]. This process resulted in higher resolution systems that were made by hydrating higher resolution model cement particles. A second way of preparing higher resolution systems was to take the original 100^3 microstructure and sub-divide each voxel. In this way, a better elastic solution was obtained but on the same microstructure. For example, a narrow one-voxel neck would now be represented by several voxels, thus allowing more elastic freedom in that neck. The elastic moduli code was then run on each system. For systems larger than 100^3, a parallel version of the code was used, and run on parallel computer clusters at NIST [13].

Fig. 7 shows the values of E and G for a w/c=0.6, α=0.219 early age cement paste, plotted vs. the system size N, which represents the number of voxel lengths in the 100 μm physical length of the side of the computational unit cell. The resolution scaling here was of the first kind, actually changing the resolution at which the cement particles were

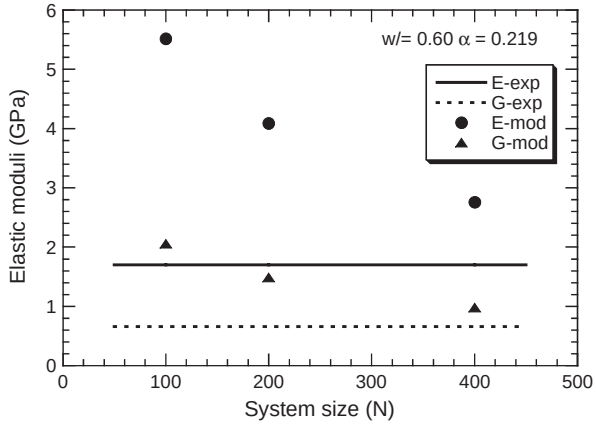

Fig. 7. Elastic moduli of cement paste system (w/c=0.60, α=0.219) for the L cement, plotted against the number of voxels per 100 μm in the model. The straight lines are the experimental values, and the points are from numerical computations.

made and altering the CEMHYD3D model so as to accurately scale with system resolution [44]. The computed elastic moduli values decrease rapidly with N, and one might guess from the graph that with increased resolution, the values are asymptotically approaching the experimental values. When the resolution was also altered the second way mentioned above, by simply sub-dividing each voxel in the original 100^3 microstructure and keeping the same properties from "parent" to "daughter" voxel, similar results were obtained (not shown), implying that scaling the hydration to different resolutions was done correctly and did not introduce any extra unphysical artifacts. Previous work on scaling the resolution may have introduced some unphysical artifacts [8].

A more detailed comparison to experiment is illuminating for the above case. For this w/c=0.6, α=0.219 cement paste, the experimental elastic moduli values are E=1.7 GPa and G=0.66 GPa (both with uncertainties of at least +5%, since it can be difficult to make early material age resonance measurements). Note that actual measurements were made at degrees of hydration before and after this value of the degree of hydration, so that the experimental results quoted are only a linear interpolation. Computing the corresponding value of K, the bulk modulus, and ν, the Poisson's ratio, one obtains ν=0.29. Choosing the value of E to be 5% higher and the value G to be 5% lower, one obtains ν=0.423, so that the value of Poisson's ratio obtained at this early age is quite sensitive to the values of E and G used, since they are so small compared to later ages. There is some early age white cement paste data in the published results and thesis of Boumiz [34]. At a w/c ratio of 0.6 and approximating the degree of hydration from the thesis graph, we obtain $E \approx 1.0$ GPa, $G \approx 0.35$ GPa, and $\nu \approx 0.47$. The best simulation values, for the 400^3 system, are E=2.76 GPa and G=0.98 GPa, with ν=0.408. Our experimental value of ν=0.29 then seems much too low for such an early age material and so it is probably true that the real result has been masked by the uncertainty and the

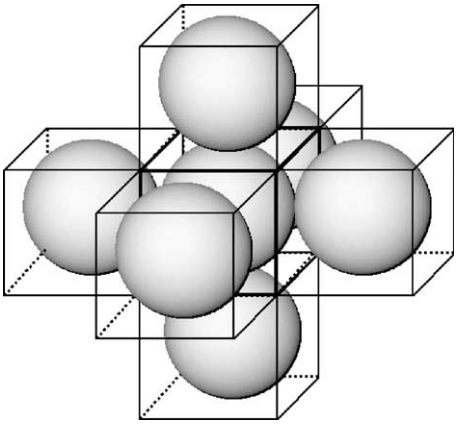

Fig. 8. Illustration of sphere in a periodic box microstructure. The periodic reflections to the top and bottom, left and right, and front and back, are shown to help picture the full 3-D structure.

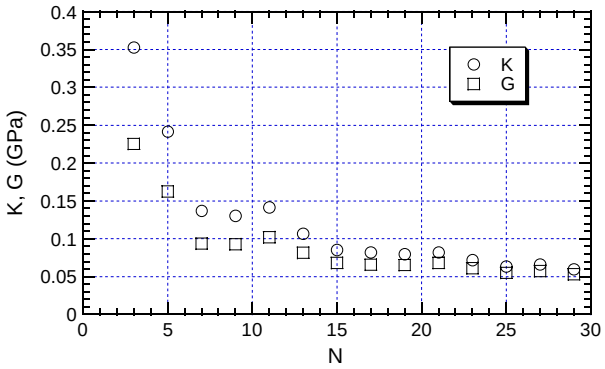

Fig. 9. How stiffness of spherical particle–spherical particle contact can decrease with increasing values of N (N=number of voxels per box length D, N/D=resolution, D is fixed). Image of touching spheres was re-made at each increased resolution.

interpolation. After all, before set, the value of ν starts from about 0.5, the value for a liquid, and decreases from that point as hydration proceeds [34].

One might also wonder if early age C–S–H has different elastic properties than what has been determined for later age C–S–H. The 400^3 results of Fig. 7 were re-run using a value for the Young's modulus of the C–S–H phase that was three times lower. The overall elastic moduli then became E=1.72 GPa and G=0.6 GPa, so that ν=0.43. So it is possible that a lower value of Young's modulus for early age C–S–H is a real effect, since it brings the 400^3 simulation results down toward more physical values. However, if early age C–S–H is similar to the low density form of C–S–H that has been studied [5], its Young's modulus is not much lower than the high density, presumably later age form of C–S–H, 21.7+2.2 vs. 29.4+2.4 GPa [5]. A combination of more nano-indentation experiments and careful early age resonance data combined with high-resolution modeling can perhaps resolve this question.

The more general question for the simulation results is – why this dependence of elastic moduli on digital resolution? At much higher degrees of hydration, one can check to see if digital resolution matters; it does not. At early hydration age, the microstructure, after set, is connected primarily by thin, incomplete, random surface layers of C–S–H and perhaps ettringite linking the cement particles. A simple test case can

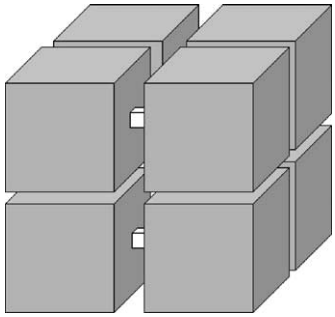

Fig. 10. Illustration of part of the microstructure of a cube linked by a single voxel to other cubes in a periodic box.

illustrate this early age cement paste behavior, showing how as an entire microstructure is represented at higher and higher resolution, the elastic moduli are reduced. Take the microstructure consisting of a single sphere, centered in a cubic box, whose diameter D is equal to the side length of the box. With periodic boundary conditions, a true continuum sphere touches six other spheres at point contacts (see Fig. 8). This system will have a finite bulk modulus, since the spheres may push against each other, but a zero shear modulus, since point contacts cannot offer resistance to shear forces. The system is approximated by 3-D digital images, of fixed physical size D. As the number of voxels, N, on a side becomes larger, the system is better resolved with more voxels per unit length (N/D), allowing the digital spheres to look more and more spherical. At low values of N/D, where N is only 3, for example, a diameter=3 voxel sphere is simply a $3\times3\times3$ cube with the eight corner voxels removed. The sphere-to-sphere interface will be made up of five voxel faces locked together, so the system will be quite stiff, both in K and in G. As the resolution N/D increases, the contact will become smaller and smaller with respect to the spheres, and so the elastic moduli should go down. Fig. 9 shows just this behavior, which is illustrative of the cement paste system. As N/D becomes infinite, the shear modulus should go to zero (neglecting any frictional forces and assuming no simultaneous compression), because of the point contacts, while the bulk modulus should asymptote to a finite value. This microstructure has cubic symmetry, so its three independent moduli, C_{11}, C_{12}, and C_{44}, have been averaged to obtain an isotropic bulk modulus and shear modulus [17,25,26].

Unlike the early cement paste model systems studied, the sphere system shown in Fig. 8 will not have significantly smaller moduli when the original microstructure at $N=D=3$ is simply sub-divided. Fig. 10 shows a slightly different system, a cube periodically linked on all six sides by one-voxel connections to identical cubes. As this microstructure is sub-divided, the single-voxel connections become multiple-voxel connections, 2^3, 4^3, and finally 8^3 voxels in extent, causing the elastic moduli to decrease, since having more voxels in the connection allows for more flexibility in the connection and hence lower values of elastic moduli. The cube was originally 7^3 voxels in size when only one connecting voxel was used. Fig. 11 shows the results for the computed elastic moduli vs. the side length of the microstructure in terms of voxels (N). The cubic moduli have been averaged to obtain isotropic bulk and shear moduli. The drop in modulus is not as dramatic as in Fig. 9, since in the limit of infinite resolution, where the physical length per voxel goes to zero, the moduli will be non-zero, while in the sphere microstructure shown in Fig. 8, the shear modulus goes to zero.

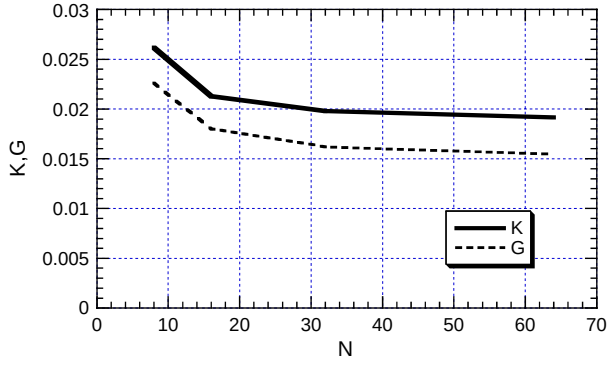

Fig. 11. How the bulk and shear moduli of this figure's microstructure can decrease with increasing resolution (original microstructure was simply sub-divided).

5. Elastic moduli fractions

It has been mentioned above, qualitatively, how the cement particle phase might contribute to the overall elastic moduli at early hydration age. It is interesting to study quantitatively how each major phase contributes to the overall elastic moduli. One can develop a measure of this analytically. The overall elastic moduli are found by averaging each component of the stress tensor and strain tensor over the entire microstructure:

$$<\sigma_{ij}> = \frac{1}{V}\int \sigma_{ij}\mathrm{d}V$$

$$<\varepsilon_{ij}> = \frac{1}{V}\int \varepsilon_{ij}\mathrm{d}V \qquad (2)$$

and defining the effective elastic moduli via

$$<\sigma_{ij}> = C^{\mathrm{eff}}_{ijkl} <\varepsilon_{kl}> \qquad (3)$$

If one wants all the individual components of the elastic moduli tensor, then one can apply one component of the strain tensor at a time [17]. The average strain tensor is equal to the strain tensor applied to the periodic unit cell of the cement paste model [2–4]. One can then read off the components of the effective elastic moduli tensor by dividing the appropriate components of the average stress tensor by the value of the average strain. We can rewrite Eq. (2) for the average stress tensor by:

$$<\sigma_{ij}> = \sum_{m=1}^{N} c_m \frac{1}{V_m}\int_m \sigma_{ij}\mathrm{d}V = \sum_{m=1}^{N} c_m <\sigma_{ij}>_m \qquad (4)$$

where the subscript m indicates the mth distinct chemical phase out of N total phases, the integral is now taken only over the volume of the mth phase, and c_m is the volume fraction of phase m. We can compute the partial contributions of each phase to the overall effective elastic moduli, and express them as a fraction of the total elastic moduli. We can then write:

$$K^{\mathrm{eff}} = \sum_{m=1}^{N} c_m <K>_m$$

$$G^{\text{eff}} = \sum_{m=1}^{N} c_m < G >_m \tag{5}$$

where $<K>_m$, for example, represents the average bulk modulus, as defined by Eq. (4), in phase m. Dividing both sides of Eq. (5) by the effective property, we then obtain

$$1 = \sum_{m=1}^{N} c_m k_m$$

$$1 = \sum_{m=1}^{N} c_m g_m \tag{6}$$

where now the fraction of the bulk modulus supplied by phase m is equal to the product of c_m, the volume fraction of phase m, and a coefficient k_m. A similar relation holds for the shear modulus.

To analyze how each phase fraction contributes to the overall elastic moduli, we have used the late age D cement results. Fig. 12 shows the results, broken down into five parts. Graph (a) shows how the phase volume fractions vary with w/c ratio. The saturated pores and the residual cement vary the most, while the CH and C–S–H phases are fairly flat vs. w/c ratio. The cement phase includes only remnant clinker phases – C_3S, C_2S, C_3A, and C_4AF. All other phases, including any residual form of gypsum phase, are included in the "other" phase. This joint phase must be fairly flat vs. w/c, since the rise in the saturated porosity with increasing w/c ratio approximately cancels out the corresponding decrease in residual cement, and the CH and C–S–H phase are, as said above, also fairly flat with w/c. Graph (b) shows how each of these five phases contribute to the overall bulk modulus, as a function of w/c ratio. At the lowest w/c ratios, the residual cement can contribute up

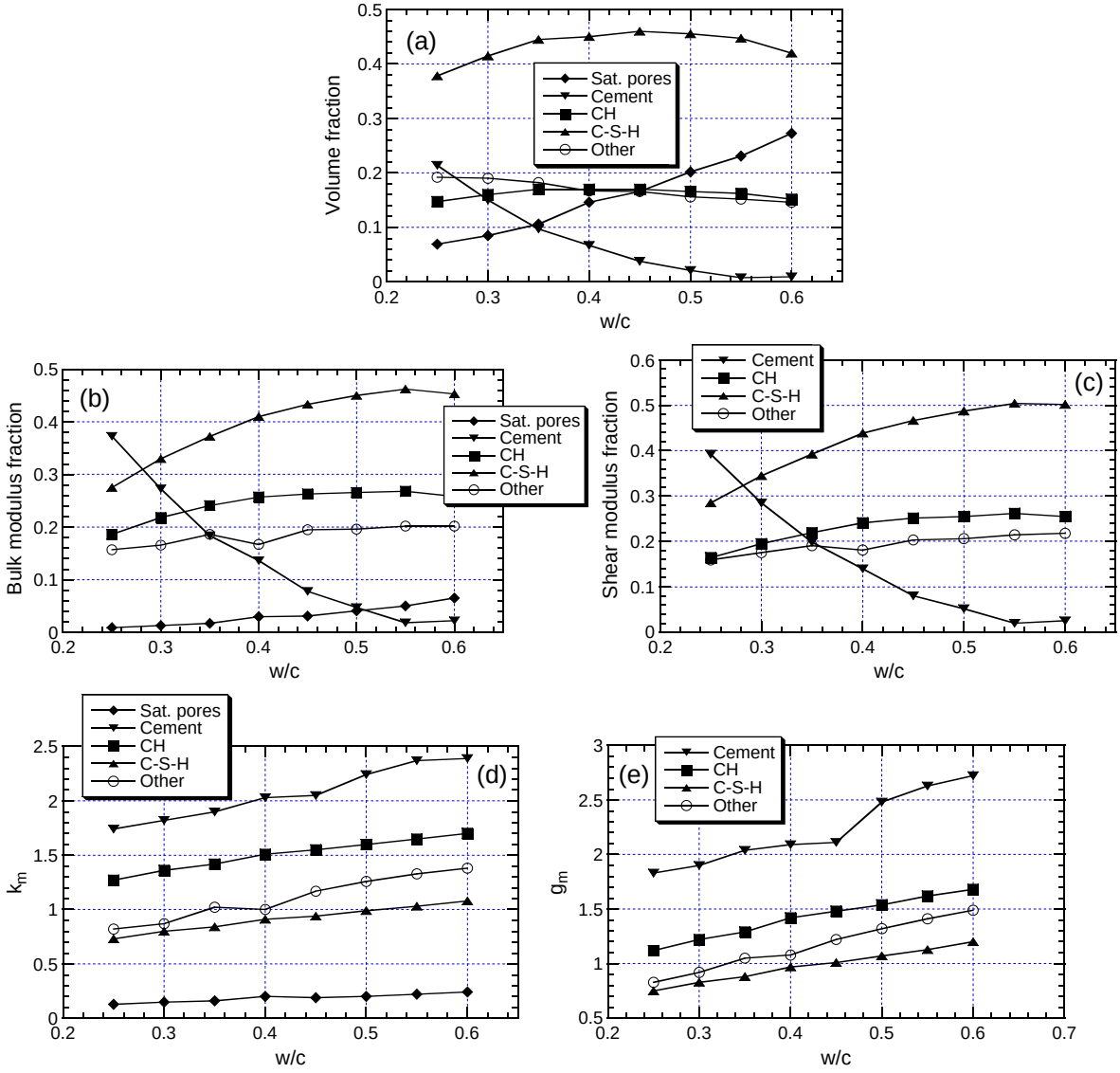

Fig. 12. (a) Volume fractions of phases, fractional phase contributions to (b) bulk and (c) shear moduli, and phase volume fraction coefficients for (d) bulk and (e) shear moduli, for the D cement at late ages of hydration over a range of w/c ratios.

to 40%. At the highest values of w/c ratio, the C–S–H phase contributes the most, about 45%, while the saturated porosity now contributes about 6%. Remember that the water in the saturated porosity has a bulk modulus of 2.0 GPa, so it can contribute to the bulk modulus in dynamic modulus measurements. The CH phase contributes between 20% and 30% over all the range of w/c ratios studied, so it has to be classified as a major contributor to the bulk modulus. Fig. 12c shows how each phase contributes to the overall shear modulus. The saturated porosity is of course missing from this graph, as the water cannot sustain a shear stress, so it cannot contribute to the shear stress average over the microstructure. At the lowest w/c ratio, w/c=0.25, the residual cement contributes 40% of the shear modulus, the C–S–H 28%, and the CH and the "other" phase each contribute about 16%. The contributions of the CH and "other" phase both increase slightly with w/c ratio, but the contribution of the C–S–H phase rises to 50%, while the residual cement contribution falls off to near-zero since the volume fraction of residual cement also decreases sharply.

There is an additional composite theory concept needed first before Fig. 12d and e can be discussed. The question to consider is – what is the value of the coefficients k_m (g_m) in Eq. (6)? In general, these coefficients can only be exactly known if the complete elastic solution for a random composite system were known, which is usually not the case. But in the dilute limit, these coefficients are exactly known, at least up to first order in volume fraction. For simplicity, consider the bulk modulus of a two phase composite, where both phases are elastically isotropic. When only a dilute amount of phase 2 is present, the composite bulk modulus K^{eff} can be written exactly as a power series in c, the volume fraction of phase 2 [2,3],

$$K^{\text{eff}} = K_1(1 + [K]c) + O(c^2) \tag{7}$$

where K_i is the bulk modulus of phase i, and $[K]$ is the intrinsic bulk modulus that depends on the shape of the phase 2 inclusion and the ratio K_2/K_1 [2,3,41–43]. If one rewrites Eq. (7) slightly, dividing both sides by K^{eff} and showing the phase contributions more clearly, then up to first order in c one has exactly

$$1 = \frac{K_1(1-c)}{K^{\text{eff}}} + \frac{(K_1 + [K])c}{K^{\text{eff}}} \quad \text{or} \quad 1 = k_1 c_1 + k_2 c_2 \tag{8}$$

where $c_1 = 1 - c$ and $c_2 = c$. Eq. (8) looks exactly like Eq. (6), except that now the coefficients k_1 and k_2 are known exactly: $k_1 = K_1/K^{\text{eff}}$ and $k_2 = (K_1 + [K])K^{\text{eff}}$. Each term consists of a factor, defined as k_m, times the volume fraction of that phase, as in Eq. (6). Now consider the second part of Eq. (8). It is known that if $K_1 = K_2$, then $[K] = 0$ [42]. In that case, the factor for phase 2, k_2, which multiplies the phase 2 volume fraction, c_2, is then equal to 1, and so is k_1, since in this case $K^{\text{eff}} = K_1$. Though Eq. (8) becomes a trivial identity, this exercise does show that the coefficients k_m become equal to one when the bulk modulus of a phase equals the overall effective bulk modulus. In the general, multi-phase case, we have Eq. (6).

When the factors k_m and g_m are computed for a general composite, we might expect that the case when $K_m = K^{\text{eff}}$ might be an important point for the value of k_m. In particular, the factors k_m could have the property that $k_m = 1$ when the moduli of the mth phase equals the overall moduli, which is taken to be the effective "matrix phase." There is no reason to expect, however, that an exact result from the dilute limit will still hold in the multi-phase, non-dilute limit.

Fig. 12d shows the values of k_m and the equivalent quantities for the shear modulus, g_m, are plotted in Fig. 12e. All the values increase with w/c ratio, as the overall elastic moduli decrease. It is known that intrinsic moduli always increase as the ratio of the elastic moduli of the inclusion to the matrix phase increases. These quantities do the same. The phase elastic moduli are fixed, so as the "matrix" moduli decrease, the ratio increases. In Fig. 12d, only the C–S–H and the "other" phase cross the value of 1. The C–S–H phase crosses the value of 1 at a w/c ratio of approximately 0.5. The bulk modulus of the cement paste at this point is $K = 15$ GPa, which is quite close to the value of the bulk modulus for C–S–H, $K = 14.9$ GPa (see Table 1). In Fig. 12e, again only the C–S–H and "other" phases cross the value of 1. The C–S–H phase coefficient crosses unity at w/c=0.45. The cement paste shear modulus at w/c=0.45 is $G = 8.7$, remarkably close to the C–S–H phase value of 8.96 GPa (see Table 1). The "other" phase is a conglomerate of phases, some having CH-like elastic moduli and some having C–S–H-like elastic moduli, so it makes sense that the average stiffness of this phase is somewhat greater than that of C–S–H. Therefore the lines for this phase cross the value of 1 in Fig. 12d and e at values of w/c less than that for C–S–H.

Fig. 12d and e also shows that the values for CH and cement are always greater than 1. The largest cement paste moduli computed in these results was $K = 24.8$ GPa and $G = 13.5$ GPa, at w/c=0.25, 56 d. The CH elastic moduli are $K = 40$ and $G = 16$, while those for cement are $K = 105$ and $G = 45$, all greater than the cement paste. Therefore the lines for these phases never cross 1.

If we think of the phase parameters above as something like intrinsic moduli, it is known that as the shape of an inclusion deviates from a sphere, the intrinsic moduli will increase [42]. Fig. 13 shows the cross-sections of the L cement paste microstructures at late age hydration, where nearly full hydration has been achieved. The remnant cement particles in the lower w/c ratio pastes look less spherical than those shown for the 56 d D cement pastes in Fig. 4. It is possible that these phase parameters could be higher in the late age L cement pastes because of this shape factor. This was checked, and it was found that the phase parameters for the L cement were only slightly larger than

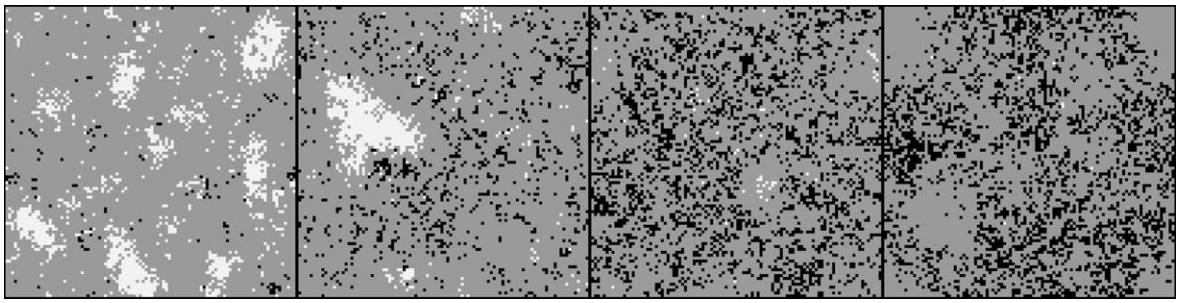

Fig. 13. Microstructural slices for the simulated L cement pastes at nearly full hydration. From left: w/c=0.25, w/c=0.35, w/c=0.50, and w/c=0.60. Gray scale is similar to that in Fig. 4.

those for the D cements, in the expected direction, but not larger than the probable numerical uncertainties.

6. Discussion and future work

Using the finite element code to compute elastic moduli involves some assumptions, some of which are operative at all material ages, and some of which are only important for early age materials. The first general assumption that is operative at any material age is that cement paste is a linear elastic material, since the code is purely linear elastic. To the extent that cement paste is not a linear elastic material, the code will not accurately predict elastic properties. However, experiment does seem to show that cement paste is generally a linear elastic material [45], at least for short durations of loading. Second, it is quite possible that the elastic moduli of the C–S–H phase changes with time as the mutual proportion of low density and high density C–S–H changes [5,6]. This is not taken into account in the model results – the same elastic moduli for C–S–H are taken for all material ages. This could be easily changed, but there is insufficient good data at present to justify such a change. Third, the CEMHYD3D microstructure is not a perfect representation of true cement paste microstructure. The smallest capillary pore size, for example, is no smaller than the voxel size. Critical capillary pores at later material ages that control fluid flow are known to be at the 0.1 μm or smaller size [46]. So, for example, fluid permeability computations will be much too high, roughly by the square of the ratio of voxel size to the critical cement paste pore diameter [47]. But elastic moduli are much more controlled by the solid frame, not the pores, so accurate elastic moduli should be able to be computed, as has been seen in this paper.

At early material ages, the viscoelastic nature of cement paste probably should not be ignored, especially at degrees of hydration smaller than the ones we are using. It is true that the resonant frequency method experimental results also ignored the viscoelastic nature of the cement paste at early ages. However, this would tend to make the measured elastic moduli frequency-dependent and higher than they really are [48], not lower. At early material ages, when the solid frame is much more tenuous, it is clear that a higher resolution (less length per voxel) should be used. Low resolution in the model can mean that particles of different phases can be touching at a corner or edge and be elastically connected, even though, with higher resolution, these particles would become physically disconnected. There are also probably more important effects like those illustrated in Figs. 8 and 10. Digital resolution scaling [16–20] has been studied for other models, and needs to be better studied in the CEMHYD3D model for elastic properties. The results in this paper related to digital resolution at early material ages are preliminary only. A more complete study of early age phenomena should include methods to more accurately model the kinetics of hydration at early ages – the dissolution bias mentioned earlier [11] is an incomplete example of what needs to be done. But for now, accurate predictions of cement paste moduli are limited to degrees of hydration above about 50% hydration, for w/c >0.45, and above a lower degree of hydration for accurate results at lower w/c ratios. It is possible that insight could be gained into the topology of early age hydrated structures using the Visual Cement Database [49].

Finally, an advantage of this approach of combining CEMHYD3D microstructures with finite element solvers is that detailed stress–strain information is available for each phase. A two-phase composite, exact dilute limit result for the coefficient of the phase volume fraction (Eq. (6)) was shown to approximately hold true in the multi-phase, concentrated case. This was an unexpected result, and probably holds true generally for any reasonable multi-phase composite, not just cement paste.

No one questions that the cement paste microstructure is complicated. Seeing how each phase, for different w/c ratios and degrees of hydration, contributes to the overall elastic response, should give new insight into experimental results and help clarify the microstructure–elastic property relationships of cement paste, which is one of the fundamental goals of materials science.

Acknowledgments

We would like to thank the members of the Virtual Cement and Concrete Testing Laboratory and the NIST HYPERCON project for partial support of this work. We would also like to thank D.P. Bentz for processing cement

data, for translating the original elastic code from Fortran to C, and for useful discussions. We thank P.E. Stutzman for imaging the L cement so that it could be added to the Virtual Cement and Concrete Testing Laboratory cement database. We thank A. Boumiz for supplying a copy of his thesis and original cement paste elastic data. We thank C. Vernet for useful conversations about the elastic properties of cement paste.

References

[1] A.M. Neville, Properties of Concrete, Fourth and Final Edition, J. Wiley and Sons, New York, 1996.
[2] S. Torquato, Random Heterogeneous Materials: Microstructure and Macroscopic Properties, Springer-Verlag, New York, 2002.
[3] G.W. Milton, The Theory of Composites, Cambridge University Press, Cambridge, 2002.
[4] R.M. Christensen, Mechanics of Composite Materials, Krieger Publishing Co., Malabar, FL, 1991.
[5] G. Constantinides and F.-J. Ulm, The effect of two types of C–S–H on the elasticity of cement-based materials: Results from nano-indentation and micromechanical modeling submitted for publication to Cem. Conc. Res. 2003.
[6] O. Bernard, F.-J. Ulm, E. Lemarchand, A multiscale micromechanics—hydration model for the early-age elastic properties of cement-based materials, Cem. Concr. Res. 33 (2003) 1293–1309.
[7] D.P. Bentz, Three-dimensional computer simulation of Portland cement hydration and microstructure development, J. Am. Ceram. Soc. 80 (1997) 3–21.
[8] E.J. Garboczi, D.P. Bentz, The effect of statistical fluctuation, finite size error, and digital resolution on the phase percolation and transport aspects of the NIST cement hydration model, Cem. Concr. Res. 31 (2001) 1501–1514.
[9] E.J. Garboczi, J.W. Bullard, Particle shape of a reference cement, Cem. Concr. Res. 34 (2004) 1933–1937.
[10] E.J. Garboczi, Three-dimensional mathematical analysis of particle shape using X-ray tomography and spherical harmonics: application to aggregates used in concrete, Cem. Concr. Res. 32 (2002) 1621–1638.
[11] J.W. Bullard, Modeling the hydration kinetics of fine cements: application to CEMHYD3D, submitted to Cem. Con. Res. (2004).
[12] E.J. Garboczi, Finite Element and Finite Difference Programs for Computing the Linear Electric and Elastic Properties of Digital Images of Random Materials, NIST Internal Report 6269 (1998) Also available at http://ciks.cbt.nist.gov/monograph/, Part II, Chapter 2.
[13] R.B. Bohn, E.J. Garboczi, User manual for finite element and finite difference programs: a parallel version of NIST IR 6269, NIST Internal Report 6997 (2003).
[14] E.J. Garboczi, A.R. Day, An algorithm for computing the effective linear elastic properties of heterogeneous materials: 3-D results for composites with equal phase Poisson ratios, J. Mech. Phys. Solids 43 (1995) 1349–1362.
[15] A.P. Roberts, E.J. Garboczi, Elastic properties of a tungsten–silver composite by reconstruction and computation, J. Mech. Phys. Solids 47 (1999) 2029–2055.
[16] A.P. Roberts, E.J. Garboczi, Elastic properties of model porous ceramics, J. Am. Ceram. Soc. 83 (2000) 3041–3048.
[17] S. Meille, E.J. Garboczi, Linear elastic properties of 2-D and 3-D models of porous materials made from elongated objects, Mod. Sim. Mater. Sci. Eng. 9 (2001) 1–20.
[18] A.P. Roberts, E.J. Garboczi, Elastic properties of model random three-dimensional open-cell solids, J. Mech. Phys. Solids 50 (2002) 33–55.
[19] A.P. Roberts, E.J. Garboczi, Elastic moduli of model random three-dimensional closed-cell cellular solids, Acta Mater. 49 (2001) 189–197.
[20] C.H. Arns, M.A. Knackstedt, W.V. Pinczewski, E.J. Garboczi, Computation of linear elastic properties from microtomographic images: methodology and agreement between theory and experiment, Geophysics 67 (2002) 1396–1405.
[21] Siham Kamali, Micheline Moranville, Edward Garboczi, Stéphanie Prené, Bruno Gérard, Influence of Hydrate Dissolution by Water on the Young's Modulus of Cement-Based Materials, FRAMCOS conference. October 2003.
[22] A.P. Roberts, E.J. Garboczi, Computation of the linear elastic properties of random porous materials with a wide variety of microstructure, Proc. Royal Soc. Lond. A 458 (2002) 1033–1054.
[23] S.P. Timnoshenko, J.N. Goodier, Theory of Elasticity, McGraw-Hill, New York, 1970.
[24] L.D. Landau, E.M. Lifshitz, Theory of Elasticity, 3rd Edition, Pergamon, Oxford, 1986.
[25] J.P. Watt, L. Peselnick, Clarification of the Hashin–Shtrikman bounds on the effective elastic moduli of polycrystals with hexagonal, trigonal, and tetragonal symmetries, J. Appl. Phys. 51 (1980) 1525–1530.
[26] J.P. Watt, Hashin–Shtrikman bounds on the effective elastic moduli of polycrystals with monoclinic symmetry, J. Appl. Phys. 51 (1980) 1520–1524.
[27] David R. Lide (Ed.), CRC Handbook of Chemistry and Physics, 78th Edition, CRC Press, Boca Raton, FL, 1997, pp. 6–127.
[28] M.M. Choy, W.R. Cook, R.F.S. Hearmon, J. Jaffe, J. Jerphagnon, S.K. Kurtz, S.T. Liu, D.F. Nelson, Landolt–Bornstein: numerical data and functional relationships in science and technology new series, in: K.-H. Kellwege, A.M. Hellwege (Eds.), Group III: Crystal and Solid State Physics, Elastic, Piezoelectric, Pyroelectric, Piezooptic, Electrooptic Constants, and Nonlinear Dielectric Susceptibilities of Crystals, vol. 11, Springer-Verlag, Berlin, 1979. Revised and Extended Edition of Volumes III/1 and III/2.
[29] A.S. Bhalla, W.R. Cook, R.F.S. Hearmon, J. Jerphagnon, S.K. Kurtz, S.T. Liu, D.F. Nelson, J.-L. Oudar, Landolt–Bornstein: numerical data and functional relationships in science and technology new series, in: K.-H. Kellwege, A.M. Hellwege (Eds.), Group III: Crystal and Solid State Physics, Elastic, Piezoelectric, Pyroelectric, Piezooptic, Electrooptic Constants, and Nonlinear Dielectric Susceptibilities of Crystals, vol. 18, Springer-Verlag, Berlin, 1984. Supplement to Volume III/11.
[30] G. Mavko, T. Mukerji, J. Dvorkin, The Rock Physics Handbook: Tools for Seismic Analysis in Porous Media, Cambridge University Press, Cambridge, 1998. See especially Appendix 10.3.
[31] T. Ahrens (Ed.), American Geophysical Union Reference Shelf 2: Mineral Physics and Crystallography: A Handbook of Physical Constants, American Geophysical Union, Washington, D.C., 1995, p. 56.
[32] F. Holuj, M. Drozdowski, M. Czajkowski, Brillouin spectrum of $Ca(OH)_2$, Solid State Commun. 56 (1985) 1019–1021.
[33] P.J.M. Monteiro, C.T. Chang, The elastic moduli of calcium hydroxide, Cem. Concr. Res. 25 (1995) 1605–1609.
[34] A. Boumiz, D. Sorrentino, C. Vernet, F. Cohen Tenoudji, Modelling the development of the elastic moduli as a function of the degree of hydration of cement pastes and mortars, in Proceedings 13 of the 2nd RILEM Workshop on Hydration and Setting: Why does cement set? An interdisciplinary approach, edited by A. Nonat (RILEM, Dijon, France, 1997); A. Boumiz, Thèse de Doctorat d'Acoustique Physique, Universite Paris 7 (Denis Diderot) (1995).
[35] K. Velez, S. Maximilien, D. Damidot, G. Fantozzi, F. Sorrentino, Determination by nanoindentation of elastic modulus and hardness of pure constitutents of Portland cement clinker, Cem. Concr. Res. 31 (2001) 555–561.
[36] R.A. Helmuth, D.H. Turk, Elastic moduli of hardened Portland cement and tricalcium silicate pastes: effect of porosity, Symposium on Structure of Portland Cement Paste and Concrete (Special Report 90), Highway Research Board, Washington, D.C., 1966, pp. 135–144.
[37] P.D. Tennis, H.M. Jennings, A model for two types of calcium silicate hydrate in the microstructure of Portland cement pastes, Cem. Concr. Res. 30 (2000) 855–863.

[38] K. Velez, S. Maximilien, D. Damidot, F. Sorrentino, G. Fantozzi, Determination by Nanoindentation of the Elastic Modulus and the Hardness of Synthetic Calcium Silicate Hydrates, 2001 (preprint).
[39] B.N. Lucas, J.C. Hay, W.C. Oliver, Using multidimensional contact mechanics experiments to measure Poisson's ratio, J. Mater. Res. 19 (2004) 58–65.
[40] T.I. Zohdi, P.J.M. Monteiro, V. Lamour, Extraction of elastic moduli from granular compacts, Int. J. Fract. 115 (2002) L49–L54.
[41] J.F. Douglas, E.J. Garboczi, Intrinsic viscosity and polarizability of particles having a wide range of shapes, Adv. Chem. Phys. 91 (1995) 85–153.
[42] E.J. Garboczi, J.F. Douglas, Intrinsic conductivity of objects having arbitrary shape and conductivity, Phys. Rev., E 53 (1996) 6169–6180.
[43] M.L. Mansfield, J.F. Douglas, E.J. Garboczi, Intrinsic viscosity and the electrical polarizability of arbitrarily shaped objects, Phys. Rev. E 64 (2001) 61401–61416.
[44] J.W. Bullard (Ed.), The Virtual Cement and Concrete Testing Laboratory: Annual Report 2003, NIST Internal Report 7096, January 2004.
[45] P.K. Mehta, P.J.M. Monteiro, Concrete: Structure, Properties, and Materials, 2nd Edition, Prentice Hall, Englewood Cliffs, NJ, 1993, p. 81. See also Ref. [1], p. 81.
[46] D.N. Winslow, C.W. Lovell, Measurements of pore size distributions in cements, aggregates, and soils, Powder Technol. 29 (1981) 151–165.
[47] A.J. Katz, A.H. Thompson, Quantitative prediction of permeability in porous rock, Phys. Rev., B 34 (1986) 8179–8181.
[48] D.R. Bland, The Theory of Linear Viscoelasticity, Pergamon, Oxford, 1960.
[49] D.P. Bentz, S. Mizell, S. Satterfield, J. Devaney, W. George, P. Ketcham, J. Graham, J. Porterfield, D. Quenard, F. Vallee, H. Sallee, E. Boller, J. Baruchel, The visible cement data set, NIST J. Res. 107 (2) (2002) 137–148. Data are available at http://visualcement.nist.gov.